RSC Advances

ROYAL SOCIETY OF CHEMISTRY

www.rsc.org/advances

Preparation and characterization of the linked lanthanum carboxymethylcellulose microsphere adsorbent for removal of fluoride from aqueous solutions

Jing Wang [a], Xiaoyan Lin [a, b,*], Xuegang Luo [a, b], Wenhui Yao[a]

[a] Department of Materials Science and Engineering, Southwest University of Science and Technology, Mianyang, Sichuan 621010, China

[b] Engineering Research Center of Biomass Materials, Ministry of Education, Mianyang, Sichuan 621010, China

Abstract: Linked Carboxymethyl cellulose microsphere loaded with lanthanum (III) (linked-CMC-La) were fabricated by glutaraldehyde linked lanthanum carboxymethyl cellulose microspheres (CMC-La) and used to remove fluoride from aqueous solution. Characterizations of SEM, resistance to acid and alkali, TG, pH_{pzc} and FT-IR were used to distinguish the superiority of the two adsorbents. Results showed that the linked CMC-La had a higher decomposition temperature (200℃) than CMC-La (190℃) and a better resistance to acid and alkali compared with CMC-La. Batch adsorption experiments were also performed on factors of pH, initial fluoride concentration, and contact time. Results showed that the maximum removal efficiency (*RE*) of CMC-La and linked CMC-La were about 98.85 % and 99.31 %, respectively, when the fluoride concentration was 40 mg/L at pH 4.0. Adsorption process could be well described by Langmuir isotherm model. The adsorption kinetics data was[1] well fitted pseudo-second-order model. The analysis of adsorption and desorption of linked

* Corresponding author. Tel: +86 0816 6089372, Fax: +86 0816 6089372.
Email address: lxy20100205@163.com (X. Lin)

CMC-La and CMC-La revealed that crosslink had no obvious effect on the removal efficiency and mechanism of adsorption and desorption of two absorbents. The surface adsorption happened between linked CMC-La and fluoride due to Lewis acid-base interaction and doped with electrostatic attraction.

Keywords: carboxymethyl cellulose sodium; La (III); crosslink; fluoride; adsorption;

1. Introduction

Fluorine was a trace element necessary for human body [1]. However, when concentration was above 1.5 mg/L, fluoride can lead to many health issues, such as mottling of teeth, thyroid disorder, fluorosis of skeleton, and neurological damage [2-4]. Therefore, removal of fluoride from water source was necessary. Up to now, defluoridation had been achieved by adsorption [5], precipitation [6], donnadialysis [7], ion exchange [8], membrane separation [9] and electrodialysis [10]. Among these, adsorption was considered as one of the most convenient and economical methods for wastewater, especially for low concentration wastewater [11].

However, the viability of adsorption technique greatly depended on the adsorbents [12]. According to the adsorbent materials, adsorption could be divided into rare earth adsorption [13], bone charcoal adsorption [14, 15], aluminum salt adsorption [16] and biosorption [17]. Biosorption was chosen as one of the most promising methods due to its environmentally-friendly properties.

Lanthanum showed high affinity for fluoride ions [18]. Various adsorbents, such as gelatin [19], chitosan beads [20] and *Sarfassum* sp. [21] loaded with La (III) were

used for the purpose of fluoride removal. Microsphere adsorbent such as synthetic resins [22] was also widely used for fluorine removal by loading La (III). In this present work, carboxymethyl cellulose sodium (CMC) was chosen as the new microsphere biomaterial because of its abundant resource [23] and large amount of active groups such as hydroxy and carboxyl. And the active groups had the tendency to form complex with metal ions and crosslinking agent [24]. Though the carboxymethylcellulose loaded with only metal ions had good adsorption capacity of fluoride [25], it did not show good deeds in mechanical properties and acid and alkali resistance, which limited its possible application. Cross-linkers were usually used to modify chemical structure and textural properties of polymer by intermolecular and intramolecular linking to improve its properties.

In this study, we attempted (i) to make carboxymethylcellulose as matrix together with lanthanum to prepare the adsorbent of CMC-La microsphere and glutaraldehyde was chosen as crosslinking agent to improve the thermostability and acid and alkali resistance of the CMC-La microsphere, (ii) to characterize the difference between the two adsorbents of CMC-La and linked CMC-La, (iii) and to deduce the mechanism of the adsorption and desorption process of fluoride.

2. Material and Methods

2.1. Reagents

CMC was purchased from Aladdin Chemistry Company, Ltd. (Shanghai, China). $LaCl_5 \cdot 7H_2O$, $C_5H_8O_2$, NaF, NaOH, $C_5H_8O_2$ and HCl were purchased from Kelong

Chemicals. NaOH and HCl were prepared at the concentration of 0.05 mol L^{-1}, respectively. Besides, all reagents were analytically pure.

2.2. Microsphere preparation of CMC-La and linked CMC-La

Carboxymethyl cellulose sodium was dispersed in ultra-pure water and stirred at high speed at room temperature to form 3 % (w/v) uniform solution. Carboxymethyl cellulose sodium solution was automatically dropped into 5% (w/v) of $LaCl_5 \cdot 7H_2O$ solution using injection pump at the speed of 7.94 μm/min and the CMC-La microspheres were formed. After then, 5 mL 50%(Volume) $C_5H_8O_2$ were added into the aqueous and the linking process of microspheres stood for another 24 h, and the linked CMC-La micropheres were filtrated, washed with deionized water to remove any residual ions and dried for ten hours at 45 ℃ for further experiments.

2.3. Characterization of CMC-La and linked CMC-La

2.3.1. SEM examination of CMC-La and linked CMC-La

Morphology analysis of CMC-La and linked CMC-La was carried out by Scanning electron microscope (SEM, EVO18, Carl Zeiss, Germany). The samples were mounted on a bronze stub, sputter-coated with gold in a sputtering device for 1.5 min at 10 mA and examined at a 20 kV accelerating voltage.

2.3.2. Density and compressive resistance of CMC-La and linked CMC-La

Density (bulk density and wet true density) was measured by the experiment method. Firstly, 15mL ultrapure water was added into the 50 mL measuring cylinder and the total mass (m_1 g) was measured in the balance. Secondly, 2 mL microsphere adsorbents were added into the cylinder and m_2 (g) was attained with the same

87 balance. Thus, the mass of the samples was the difference between m_2 and m_1, namely
88 (m_2-m_1). Thirdly, the sample volume (V mL) was gained through the difference of the
89 before and after volume, too. The bulk density (g / mL) was calculated as equation (1).
90 Then, filling the cylinder with water and the total mass was m_4. Throw out the
91 adsorbent, fill the cylinder with water again and record the mass m_3. The wet true
92 density was calculated as equation (2).

93 $$d = (m_1 - m_2)/V \quad (1)$$

94 $$d_T = m_2 - m_1/(m_2 - m_1) - (m_4 - m_3) \quad (2)$$

95 Compressive resistance was one of the factors in the adsorbent application.
96 Approximately 14-15 microsphere adsorbents before dried were examined with a
97 texture analyzer (B. XTPlus, Stable Micro System Corporation, UK) [26]. A sample
98 was positioned on the stage to ensure that the probe evenly contacted the sample
99 surface. The test was performed at a constant speed of 4 mm/s and was stopped until
100 the samples were crushed to the same degree of deformation. At this time, the peak of
101 pressure force that displayed in software interface was defined as the compressive
102 strength of the samples. The final data was the average value of the 14-15
103 microspheres.

104 **2.3.3. N_2 adsorption-desorption of CMC-La and linked CMC-La**

105 N_2 adsorption and desorption experiments were conducted with a JW-BK112
106 Surface Area Analyzer and Pore Size Analyzer. The N_2 adsorption-desorption
107 isotherms could provide information of pore volume, surface area and pore size
108 distribution.

2.3.4. The resistance of CMC-La and linked CMC-La to acid and alkali

An experiment method was used to investigate the acid and alkali resistance of adsorbents. Experiments were conducted in a batch of 250 mL glass-stoppered flasks with 100 mg/L fluorine solution. Firstly, initial pH of the solution was adjusted to 1 to 12 with HCl (0.05 mol/L) and NaOH (0.05 mol/L), respectively. Secondly, 0.2 g of adsorbents were added into each flask and the flasks were shaken in an electrically thermostatic reciprocating shaker at 180 rpm for 72 h. Finally, the resistance of adsorbents to acid and alkali were attained through observing adsorbents dissolution properties at different pH.

2.3.5. Thermal properties analysis of CMC-La and linked CMC-La

The thermal stability of CMC-La and linked CMC-La were measured by thermogravimetric analysis (Q600, TA Instrument Corporation, USA). The samples were gradually heated at a rate of 20°C/min from 20 to 800 ℃ which were under protection of N_2 with a flow rate of 20 mL/min.

2.3.6. Analysis on the point of zero charge of the adsorbent

A solid addition method [27] was used to investigate the point of zero charge (pH_{pzc}) of adsorbents. Experiments were conducted in a batch of 50 mL glass-stoppered flasks containing 0.1 mol/L KNO_3. Firstly, initial pH (pH_i) of the KNO_3 solution was regulated from 3 to 11 with HCl (0.05 mol/L) and NaOH (0.05 mol/L). Secondly, 0.1 g of adsorbents were added into each flask and the flasks were shaken in an electrically thermostatic reciprocating shaker at 180 rpm for 48 h. Finally, pH of those solutions (pH_t) was detected. The difference value between pH_t and pH_i

(ΔpH = pH_i - pH_t) was plotted versus pH_i, and intersection between the curve and abscissa was pH_{pzc}.

2.3.7 **Fourier transform-infrared spectra (FT-IR) analysis**

Both CMC-La and linked CMC-La were measured by Fourier transform-infrared spectrometer (Nicolet-6700, USA) in the wavenumber range of 400-4000 cm^{-1}. Prior to the measurement with FT-IR, adsorbents were taken into the oven at 55 □ for 24 h and then pressed into discs with potassium bromide.

2.4. Batch adsorption experiment for fluoride

Batch adsorption experiments were studied with various pH, fluoride concentration and contact time. Adsorption experiments were conducted in triplicate in a 250 mL stoppered conical flask containing 50 mL of fluoride solution and a certain dosage of adsorbents. Flask was shaking in an electrically thermostatic reciprocating shaker at 180 rpm for a predetermined contact time. Fluoride removal efficiency of adsorbents was evaluated by measuring the time-dependent concentrations of fluoride. The average value of the results (differences less than 3%) was used for data analysis. Besides, the pH of initial fluoride solution was adjusted by NaOH and HCl solution.

Then solid-liquid filtrated, and the filtrates were analyzed by Metrohm 881-Compact-IC-Pro using calibration curve (linear equation: $Y = 0.0158012X - 0.285042$, where Y was absorbency and X was fluoride concentration in mg/L; R^2 = 0.999). The removal efficiency (*RE*) was calculated as follows [28].

$$RE(\%) = (C_0 - C_e)/C_0 \times 100 \quad (3)$$

Where C_0 (mg/L) and C_e (mg/L) were the initial fluoride concentration and fluoride concentration after adsorption, respectively.

2.5. Regeneration experiment of the adsorbent

Desorption of the adsorbed fluorine from CMC-La and linked CMC-La was studied by static experiments. Adsorbent (0.2 g) was dispersed in a 250 mL stoppered conical flask containing 50 mL of 100 mg/L fluorine solution as mentioned in the adsorption procedure. Once equilibrium was reached, the adsorbent that loaded with fluorine was filtered out and dried. Then the adsorbent was placed in a 250 mL stoppered conical flask containing 50 mL NaOH solution for desorption. The pH of desorption solution varied from 9.0 (CMC-La) to 11.0 (linked CMC-La). Then flask was kept in an orbital shaker at 180 rpm for a 24 h period at room temperature (25 °C). The final fluorine concentration in the filtrate was detected and desorption ratio was calculated based on the removal efficiency. The maximum adsorption-desorption times of the two adsorbents was also recorded. All experiments were carried out in duplicate and showed differences less than 3%.

3. Results and Discussion

3.1. SEM

The photo and SEM micrographs of adsorbents were presented in Fig. 1. The images illustrated that the adsorbents were granular. Compared with the CMC-La (Fig. 1a), the linked CMC-La (Fig. 1b) was regular microsphere. Although, the surface of two kinds of adsorbents were marked with a number of creases (Fig. 1c and Fig. 1d),

which increased the contact area and improved ions adsorption capacity, the surface of linked CMC-La appeared more creases per surface unit of the adsorbent. The formation of a large number of folds on the surface of adsorbents may be caused by water evaporation and surface shrinking of gel pellet. More water evaporation and surface shrinking were, more creases on the surface of adsorbents and more dense texture of gel particles were. The results from Fig. 1c and Fig. 1d indicated that linking process made a contribution to shaping the adsorbents and densification of the gel particles. Compared Fig. 1c to Fig. 1e and Fig. 1d to Fig. 1f, respectively, there was no obvious change in the creases on the surface of the adsorbent, which indicated the adsorbent was relatively stable in the adsorption process.

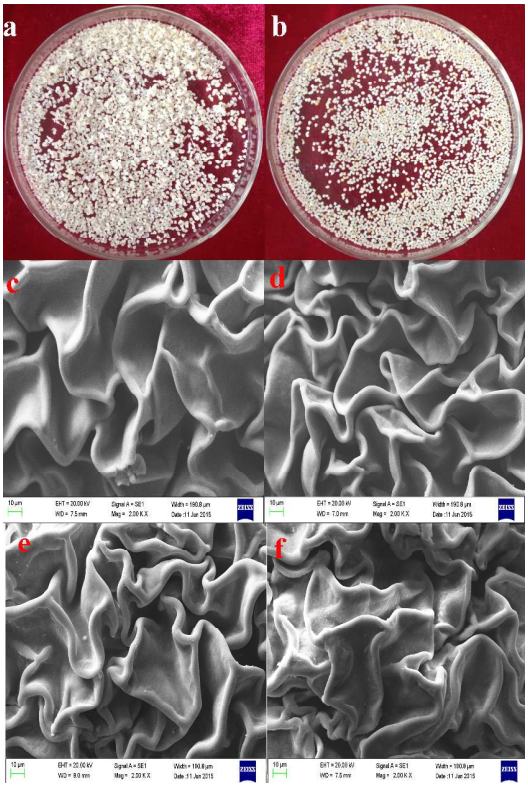

Fig.1. Photos and SEM images of adsorbents ((a) digital photo of CMC-La, (b) digital photo of linked CMC-La, (c) SEM of CMC-La, magnification × 2000, (d) SEM of linked CMC-La,

magnification × 2000 (e) SEM of CMC-La after adsorption, magnification × 2000, (f) SEM of linked CMC-La after adsorption, magnification × 2000)

3.2. Density and compressive resistance

The compressive resistance and density of adsorbents were shown in table 1. The compressive force of CMC-La was 92.125 g while the force of the linked CMC-La was 310.467 g. From this point, the linking process improved the compressive resistance of the adsorbent which may caused by densifying the gel particles. It was also consistent with conclusion of the SEM.

As for the density, both the bulk density and wet true density of the CMC-La were denser than the linked CMC-La. This may due to the heavier water absorbency of CMC-La than that of the linked CMC-La.

Table 1 Compressive resistance and density characteristics of CMC-La and linked CMC-La

Adsorbent	Force (g)	Bulk Density (g / mL)	Wet True Density
CMC-La	92.125	1.521	1.853
Linked CMC-La	310.467	1.447	1.609

3.3. N_2 adsorption-desorption of CMC-La and linked CMC-La

The results of N_2 adsorption-desorption analysis were shown in Table 2. The specific surface area of CMC-La and linked CMC-La which was calculated from the multipoint BET model was 4.132 and 1.798 m^2 /g, respectively. The total pore volume of CMC-La and linked CMC-La was 0.0036 and 0.0023 cm^3/g, respectively.

Table 2 Pore structure parameters of CMC-La and linked CMC-La

Adsorbent	Surface area (m^2/g)	Total pore volume(cm^3/g, 10^{-3})	Average pore size (nm)
CMC-La	4.132	3.6	7.051
Linked CMC-La	1.798	2.3	6.334

The pore distribution was also shown in Fig. 2. From Fig. 2, the average pore size of both the CMC-La and linked CMC-La was respectively 7.051nm and 6.334nm (Table 2), and they were mostly distributed around 6nm.

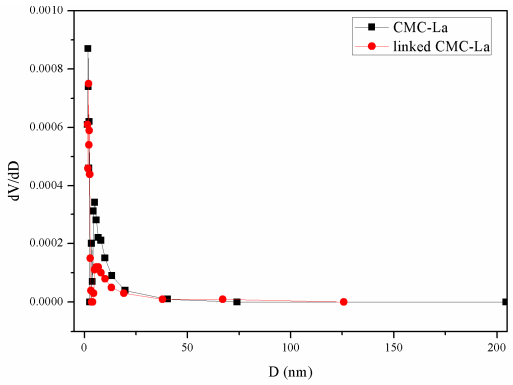

Fig. 2 The pore distribution of both CMC-La and linked CMC-La

3.4. Analysis of acid and alkali resistance

The result of the resistance of adsorbents to acid and alkali was shown in Fig.3. The previous preliminary experimental results showed that 3 to 11 of the solution pH was the critical range of the resistance of the adsorbent to acid and alkali, and 4 was the best adsorption pH for fluoride of the adsorbent. Therefore, three kinds of typical pH of 3, 4, and 11 were chosen for the acid and alkali resistance test of the adsorbent. After shaking in the solution of different pH for 72 h, the microspheres adsorbent of CMC-La were obvious swelling (Fig.3a1) when the pH value was 3 and there was no significant change except slight swelling in appearance of CMC-La when the pH was 4 (Fig. 3b1). However, the adsorbents of CMC-La decomposed (Fig.3c1) more or less when the pH value was 11 which were not microsphere any more, further lead to the adsorption solution turning to cloudy. The swelling and dissolution of the linked CMC-La at the different pH value of the adsorption solution (3, 4 and 11) were shown in Fig. 3a2, b2 and c2, respectively. Compared with CMC-La, the linked CMC-La

showed better acid and alkali resistance. There was no signal of dissolution and the adsorption solution was still clarification. From this point, the linking process improved the resistance of adsorbents to acid and alkali. This may be due to the cellulose chain interaction which was related to the presence of glutaraldehyde [29].

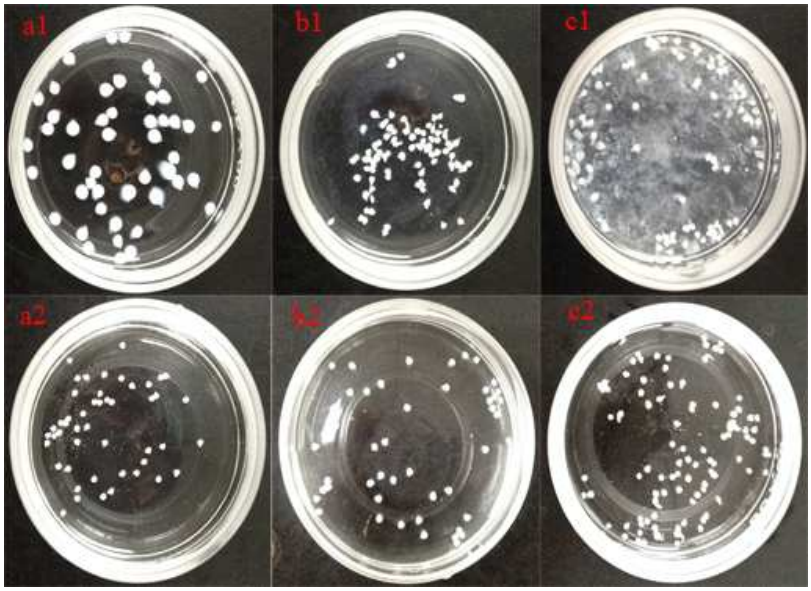

Fig.3. Digital images of CMC-La and linked CMC-La in the different pH value (a1, a2: pH 3, b1, b2: pH 4 and c1, c2: pH 11, respectively)

3.5. Thermal properties analysis

Thermogravimetric analysis was a standard of estimating the relative stability of the material according to thermal decomposition temperature. Thermogravimetric curves of CMC-La and linked CMC-La in the range of 0℃ to 800℃ were shown in Fig. 4 and DTG curve exhibited a same three-stage decomposition band in the two adsorbents. According to the DTG curve, the different decomposition process of the two adsorbents lied in the first stage that the decomposition temperature of CMC-La was 190℃ while linked CMC-La was 200℃, which was slightly higher than CMC-La. It could come to the conclusion that the cross linking made the CMC-La

more stability in the first decomposition process and the linked sites were in the hydroxyl of the carboxymethylcellulose [30]. The weight loss of both CMC-La and linked CMC-La were 45%.

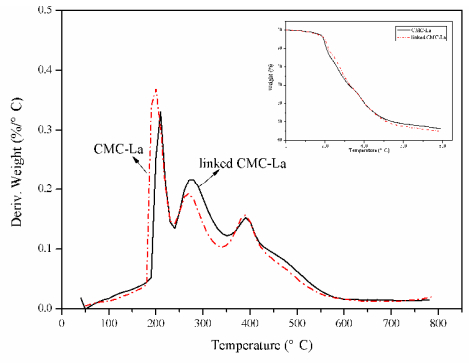

Fig.4. Thermal analysis showing TGA of adsorbent

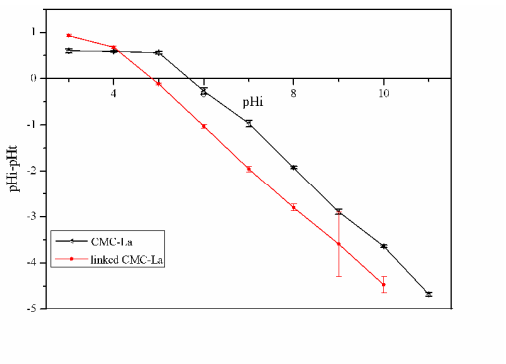

Fig.5. Determination of the point of zero charge of CMC-La

3.6. Analysis on the point of zero charge of CMC-La

The pH_{pzc} was a vital parameter to determine the net electrical neutrality in adsorbent. When pH was below pH_{pzc}, surface charge was positive [31]. Plot of pHi versus ΔpH was shown in Fig. 5. The pH_{pzc} of CMC-La and linked CMC-La in aqueous solution were at pH 5.7 and pH 4.8, respectively. So the adsorbent surface presented positive charge below pH 5.7 and pH 4.8. Therefore, electrostatic attraction between the positive adsorbent and fluoride existed below pH 5.7 and pH 4.8 [32].

3.7 Analysis of FT-IR

FT-IR spectrum of adsorbent material was presented in Fig. 6. As to CMC-La, The broad peak around 3399cm^{-1} and 1063 cm^{-1} were assigned to the stretching modes of -OH bands, and combined vibrations related to bending in -OH was observed at 1330cm^{-1} [14, 33]. Peak at 2924 cm^{-1} was due to the stretching vibration of -CH- bands [34]. The bands in CMC-La at 1590 cm^{-1} and 1423 cm^{-1} were assigned to

antisymmetric stretching and symmetric stretching of the carboxylic groups [35]. Bands between 1000 and 600cm^{-1} correspond to sugar vibrations [36]. Compared linked CMC-La with CMC-La, though faint changes, caused by linking of glutaraldehyde, in positions of individual bands such as 1587cm^{-1}, 1328cm^{-1}, 1061cm^{-1} were seen, a significant increase of bands intensity is noticeable in the wave number range 2924 cm^{-1}. It is related to the presence as well as to the formation of new C-H bonds in the considered system, which demonstrated the existing of linking process [37].

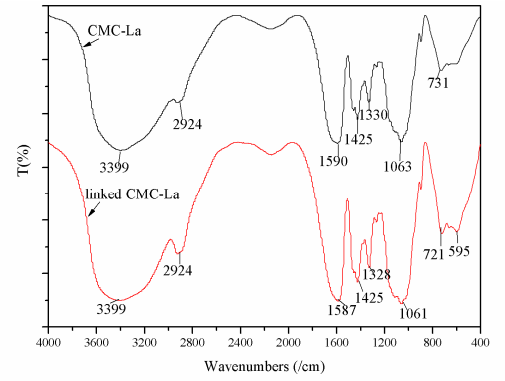

Fig. 6 FT-IR of CMC-La and linked CMC-La

3.8. Effect of pH

The effects of pH on the removal efficiency of adsorbents were studied by adjusting pH of the aqueous solution from 3 to 11 and results were shown in Fig. 7. From Fig. 7, removal efficiency decreased with the increase of the pH from 3 to 11, and the maximum removal efficiency of both CMC-La and linked CMC-La were about 93% and 98% in acid solution, respectively. In this aspect, cross-linking agent made a positive impact on the removal efficiency.

The electrostatic attraction may be the reason why removal efficiency decreased with the increase of the pH. When pH was below pH_{pzc}, surface charge was positive and the charge numbers decreased with the increase of the pH and removal efficiency decreased with the increase of the pH. When pH was above pH_{pzc}, surface charge was negative and the charge numbers increased with the increase of the pH and removal efficiency decreased with the increase of the pH. As the adsorption of fluoride happened in both acidity and basicity of aqueous solution, the electrostatic attraction may not be the only reason for adsorption of fluoride.

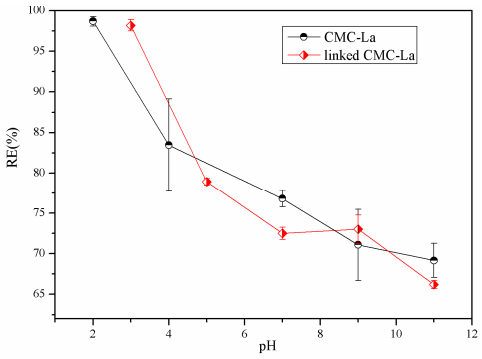

Fig.7. Effect of pH on adsorption amount and removal efficiency of CMC-La and linked CMC-La for fluoride

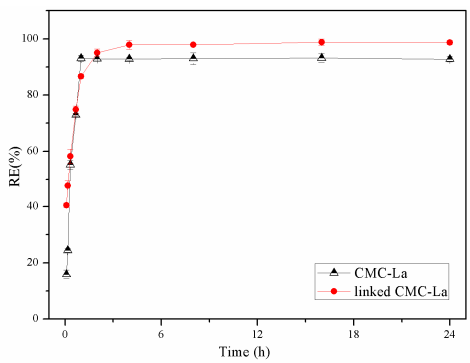

Fig. 8. Effect of contact time on adsorption amount and removal efficiency of CMC-La and linked CMC-La for fluoride

3.9. Effect of contact time and kinetics of fluoride adsorption

Effects of contact time on the adsorption by CMC-La and linked CMC-La were studied and results were shown in Fig. 8. The contact time ranged from 5 min to 24 h removal efficiency of CMC-La increased rapidly in the first 60 minutes and reached equilibrium at 60 minute while the linked CMC-La increased rapidly in the first 120 minutes and reached equilibrium at 120 minute. The equilibrium removal efficiency of CMC-La and linked CMC-La was about 93 % and 98%, respectively. And after

adsorption, both pH of the solution containing CMC-La and linked CMC-La changed to about 6.4 when the initial pH was about 4.0.

To investigate the mechanism of adsorption and its potential rate-controlling steps, different kinetic models including intra-particle diffusion models, Elovich equation, pseudo-first-order and pseudo-second-order.

The intra-paticle diffusion model was given in the following equation (4) [38].

$$Q_t = K_i t^{1/2} + C \quad (4)$$

Where *Ki* (mg/(g min $^{1/2}$)) was intra-particle diffusion rate constant and *C* (mg/g) was the intercept. The intra-particle diffusion was shown in Fig. 9. According to Eq. (4), a plot of *Qt* versus $t^{1/2}$ should be a straight line with a slope *Ki* and intercept *C* when adsorption mechanism follows the intra-particle diffusion process. For intra-particle diffusion model, it was essential for the *Qt* versus $t^{1/2}$ plots to go through the origin if the intra-particle diffusion was the sole rate-limiting step. According to Fig. 9, any plot did not pass through the origin. This indicated that although intra-particle diffusion was involved in the adsorption process, it was not the sole rate-controlling step. The sorption process tended to be followed by two phases. It was found that an initial linear portion ended with a smooth curve following by a second linear portion. The two phases in the intra-particle diffusion plot suggested that the sorption process proceeded by surface sorption and the intra-particle diffusion. The initial curved portion of the plot indicated boundary layer effect while the second linear portion was due to intra-particle or pore diffusion [39].

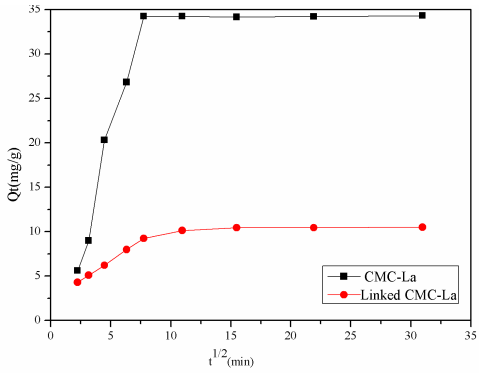

Fig.9. Intra-particle diffusion model for the adsorption of fluoride on CMC- La and linked CMC-La

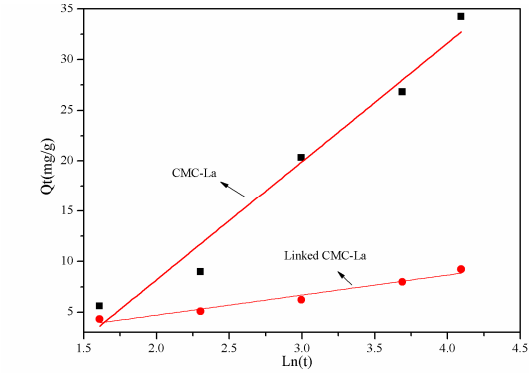

Fig.10. Elovich model for the adsorption of fluoride on CMC- La and linked CMC-La

Table 3 Parameters of pseudo-first-order kinetics, pseudo-second-order kinetics and elvoich models for fluoride removal

adsorbent	$Q_{e(exp)}$(mg/g)	pseudo-first-order kinetics			pseudo-second-order kinetics			Elovich			
		K_1 (1/min)	$Q_{e(cal)}$(mg/g)	R^2	K_2(g/mg min)	$Q_{e(cal)}$ (mg/g)	R^2	h(mg/g min)	b(g/mg)	a(mg/g min)	R^2
CMC-La	34.25	0.00421	2.21	0.222	0.0015	34.65	0.999	2.89	0.085	3.19	0.964
Linked CMC-La	26.27	0.0194	5.64	0.974	0.0099	26.58	0.999	1.12	0.51	2.89	0.955

The adsorption data was further analyzed using the Elovich models. The Elovich equation was given as follows:

$$Q_t = 1/b \ln(ab) + 1/b \ln t \quad (5)$$

where b was the initial adsorption rate (mg/g min), and the a parameter was desorption constant (g/mg). When the adsorbate ions and the surface sites interacted chemically through a second-order mechanism, the application of the Elovich equation may be more appropriate [40]. Fig. 10 showed a plot of Qt versus Ln t for the Elovich equation at 298K. The parameters of the Elovich equation were shown in Table 3. The Elovich equation described predominantly chemical adsorption on highly

heterogeneous adsorbents, but the equation did not propose any definite mechanism for adsorbate-adsorbent interaction. The coefficients were significantly depending on the amount of adsorbent with a being much more sensitive.

Then the kinetics was also investigated through Lagergren pseudo-first-order equation (6) [34] and Lagergren pseudo-second-order equation (7) [36]. The equilibrium adsorption amounts (Q_e) was calculated as equation (8). The mechanism of adsorption and its potential rate-controlling steps were also studied.

$$\ln(Q_e - Q_t) = \ln Q_e - K_1 t \quad (6)$$

$$t/Q_t = t/Q_e + 1/K_2 Q_e^2 \quad (7)$$

$$Q_e = (C_0 - C_e)V / W \quad (8)$$

$$h = K_2 Q_e^2 \quad (9)$$

Where Q_e was the equilibrium adsorption amount and Q_t was the adsorption amount when time was t. When adsorption process was equilibrium, Q_t was equal to Qe. K_1 (1/min) was the pseudo-first-order rate constant while K_2 (g/mg min) was the pseudo-second-order rate constant for fluoride adsorption process, respectively. The h (mg/g min) in equation (9) was the initial adsorption rate of the pseudo-second-order [40]. Table 3 listed the results of experimental data of the two models. From table 3, we can draw a conclusion that the adsorption process of fluoride onto both CMC-La and linked CMC-La fitted pseudo-second-order model (Fig. 11) better than pseudo-first-order model and Elovich model (Figure was not shown here). Because the calculated equilibrium adsorption amount in pseudo-second-order was almost the same as the experimental data and the R^2 was 0.999 and 0.999, respectively. R^2 was

more than those of other models. And the fast adsorption rate and short equilibrium time can also make a contribution to the result. According to the pseudo-second-order model, the rate-limiting step may be chemical sorption involving valency forces through sharing or exchange of electrons between sorbent and sorbate [37]. From this point, crosslinking of the adsorbents did not change adsorption process and the kinetics model attributed to pseudo-second-order model. It can also come to the conjecture that the linked sites by glutaraldehyde were different from adsorption sites of the adsorbents for fluorine. Because cross-linking happened between natural polymer and glutaraldehyde by linking at the amine or the hydroxyl sites [41] while ion-dipole and H-bonding were considered the primary noncovalent interactions for the adsorption [42]. Analysis of the mechanism of glutaraldehyde crosslinking CMC-La was shown in Scheme 1B of Fig.11.

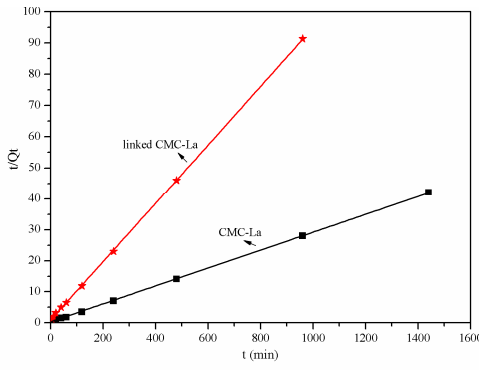

Fig.11. Pseudo-second-order kinetics model for the adsorption of fluoride on CMC- La and linked CMC-La

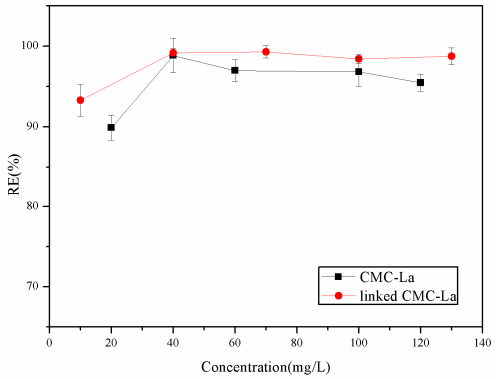

Fig.12. Effect of initial concentration on adsorption amount and removal efficiency of CMC- La and linked CMC-La for fluoride

3.10. Effect of initial concentration and isotherm models

Effects of initial concentration of fluoride on the removal efficiency onto the adsorbents were shown in Fig. 12. Fluoride concentration ranged from 10 to 130 mg/L. The removal efficiency of fluorine onto CMC-La increased with the increase of

concentration from 10 to 40 mg/L, while the removal efficiency decreased by waves from concentration 40 to 120 mg/L and the maximum removal efficiency was about 98.85% at 40 mg/L. The removal efficiency of fluorine onto the linked CMC-La increased with the increase of concentration from 10 to 40 mg/L, and stayed stable when the concentration was beyond 40 mg/L while the maximum removal efficiency was 99.31% at 40 mg/L.

Analysis of isotherm data was important for predicting the adsorption parameters. Langmuir, Freudlich, Temkin and Dubinin isotherm equations were used to identify the adsorption efficiency and the mechanism of the adsorption process. The Langmuir model can be expressed in a linear form of Equation (10) [43].

The essential feature of the Langmuir isotherm can be described by a separation factor R_L. When R_L values were between 0 and 1, the adsorption was favorable. R_L was calculated by the following equation (11) [44].

$$C_e/Q_e = 1/(K_L Q_{\max}) + C_e/Q_{\max} \quad (10)$$

$$R_L = 1/(1+K_L C_0) \quad (11)$$

The Freundlich was displayed in Equation (12) [45] and it assumed non-ideal sorption on heterogeneous surfaces [46].

$$\ln Q_e = \ln K_F + n \ln C_e \quad (12)$$

The Temkin model can be expressed in a linear form of Equation (13):

$$Q_e = RT/b_T \ln K_T + RT/b_T \ln C_e \quad (13)$$

The Dubinin model can be expressed in a linear form of Equation (14):

$$\ln Q_e = \ln Q_{max} - \beta\varepsilon^2 \quad (14)$$

β is a constant related to sorption energy ($kJ^2\ mol^{-1}$) and ε is Polanyi potential which is mathematically represented as equation (15):

$$\varepsilon = RT\ln(1+1/C_e) \quad (15)$$

Where Q_e (mg/g) was the amount of adsorbed fluoride per mass unit at equilibrium, Q_{max} (mg/g) was the theoretical adsorption capacity, K_L (L/mg) was the binding energy of the adsorption system in Langmuir, K_F (mg/g) was the Freudlich constant and n was the adsorption intensity. K_T was the Temkin isotherm equilibrium binding erengy (L/g), b_T was Temkin isotherm constant related the heat of sorption and T was the absolute temperature in Kelvin. C_0 (mg/L) and Ce (mg/L) were the initial and equilibrium concentration in solution, respectively.

The values of Langmuir, Freudlich, Temkin and Dubinin isotherm constant were obtained by linear regression method and the results were shown in Table 4. As depicted, Langmuir model was better fitted than other models (based on the higher correlation coefficient i.e. R^2 value and the Q_{max}). It indicated that the adsorption process was monolayer surface adsorption with finite number of identical sites. Fig.13 showed Langmuir model for the adsorption of fluoride on the two adsorbents. R_L values were between 0 and 1, and it indicated that the adsorption of fluoride by CMC-La and linked CMC-La was favorable [47].

Table 4 Characteristic parameters obtained by Langmuir and Freundlich equations.

adsorbent	Temperature T (K)	Langmuir constant				Freundlich constant			Temkin constant			Dubinin-Redushkevich		
		K_L (L/mg)	Q_{max} (mg/g)	R^2	R_L	n	K_F (mg/g)	R^2	b_T (J/mol)	k_T (L/mmol)	R^2	$\beta(mol^2\ kJ^{-2})$	Q_{max} (mg/g)	R^2
CMC-La	298	0.79	36.440	0.999	0.013	0.45	14.73	0.954	339.17	5.047	0.262	0.116	24.60	0.647
Linked CMC-La	298	1.21	42.662	0.906	0.008	0.52	22.51	0.840	184.53	4.884	0.622	0.089	30.75	0.834

3.11 Comparison with related adsorbent

The comparison of adsorption capacity (Q_{max}) of related adsorbents for fluoride was shown in Table 5. The results showed that linked CMC-La in this study was superior to related adsorbents in adsorption capacity. The possible reason may be the creases in surface that added the adsorption site and the adsorption capacity.

Table 5 Comparison with related adsorbent

Adsorbent	$C(F^-)$(mg L^{-1})	pH	Contact time (h)	Temperature(℃)	Qmax(mg g^{-1})	Reference
La^{3+}-impregnated gelatin	40	5-7	0.67	25	21.28	19
La-Al-loaded scoria	20.82	7.2	10	10±1	0.113	48
La-modified chitosan	10	6.7	24	25	3.5	49
Protonated chitosan beads	10	7	0.5	30	1.66	50
Zr-immobilized resin	80	3	24	30	23.18	51
granular ferric hydroxide	1-100	6-7	24	25	7.0	52
Linked CMC-La	100	3	24	25	42.66	Present study

3.12. Regeneration experiment

To keep down the cost of adsorption process, regeneration of the waste adsorbent for recycling usage was critical in industrial application. As the adsorption behavior of fluorine onto the adsorbents was much more dependent on pH value, NaOH solution was chosen as eluent and the pH of the eluent was based on the resistance of the adsorbents to acid and alkali. The pH of the eluent differed from 9.0 (CMC-La) to 11.0 (linked CMC-La), and results were shown in Fig. 14.

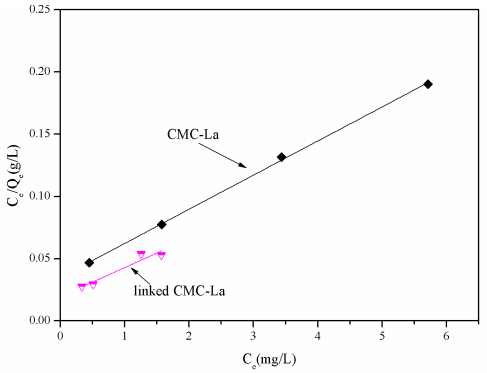

Fig. 13. Langmuir model for the adsorption of fluoride on CMC- La and linked CMC-La

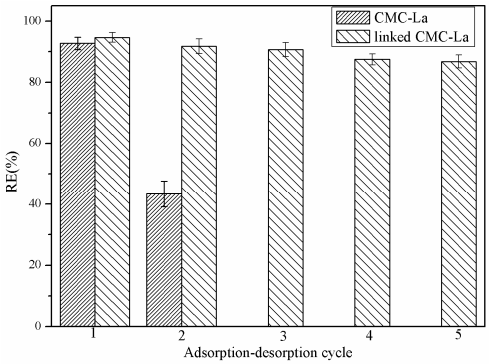

Fig.14. Adsorption-desorption cycle of CMC-La and linked CMC-La

From Fig. 14, the maximum recycle times of CMC-La was twice and the first removal efficiency was about 92 % while the second reduced to about 43 %. As for the linked CMC-La, it can regenerate at least 5 times and the removal efficiency was still above 86 %. The fluorine removal efficiency decreased only 8 %, demonstrating that the linked CMC-La in this study can be reused and recycled easily. It was significant for practical applications. From this aspect, we can also achieve the conclusion that the linking process improved the hydraulic stability of CMC-La and increased the recycle times of the adsorbent, which resulted in reducing the cost of the use of adsorbent.

3.13. Mechanism analysis of adsorption fluoride onto linked CMC-La and desorption of fluorine with alkali aqueous

As concerned for the loading process, La (Ⅲ) was loaded onto the CMC through ion exchange of sodium in CMC [53, 54]. However, the positive charge of the loaded with La (Ⅲ) was impossible to be neutralized by carboxylic groups and it needed other anionic species like hydroxyl ions existing in aqueous solution. The mechanism

of La (Ⅲ) loaded onto the linked CMC was depicted in Fig. 15 Scheme 1A. Glutaraldehyde had been used extensively as a cross-linking agent for natural macromolecule compound such as protein and methylcellulose [55]. Because it can not only react with amino group, but also react with the phenolic hydroxyl group [56]. As the linking process happened between carboxylmethylcellulose, the linking group was the hydroxyl group in CMC which was shown in Fig. 15 Scheme 1B and the space grid structure was formed to improve the adsorbents stability and resistance [57]. The denser structure was also the reason of the improvement of hydraulic stability and recycle of the linked CMC-La, compared with CMC-La.

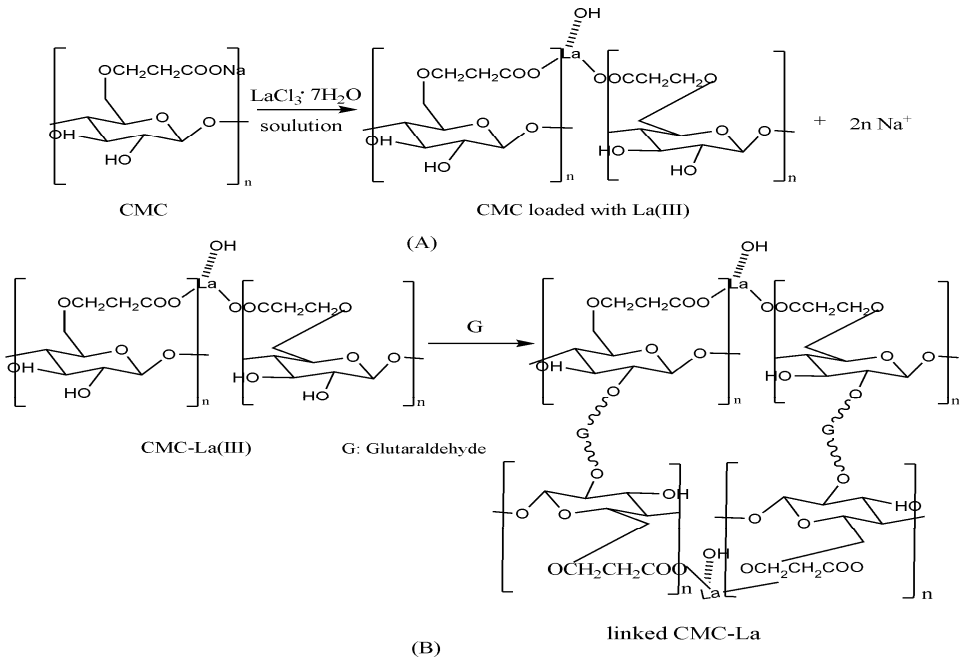

Fig.15. Scheme 1. Mechanism of preparation of linked CMC-La (A: La (III) loading process onto CMC, B: CMC-La linking process with glutaraldehyde).

After adsorption, fluoride reacted with La (Ⅲ) [58] and substituted the hydroxyl in linked CMC-La through Lewis acid-base interaction and it also explained the reason why after adsorption the pH changed to about 6.4 when the initial pH was

about 4.0. The mechanism of adsorption process was shown in Fig. 16 Scheme 2A. Besides, according to pH_{pzc}, the electrostatic attraction between positive adsorbent and fluoride below pH 4.8 was shown in Fig. 16 Scheme 2B. Thus it can be seen that adsorption sites were different from linked sites of the adsorbents. That may be the reason why the linking process had no obvious effects on the adsorption of CMC-La and linked CMC-La for fluoride.

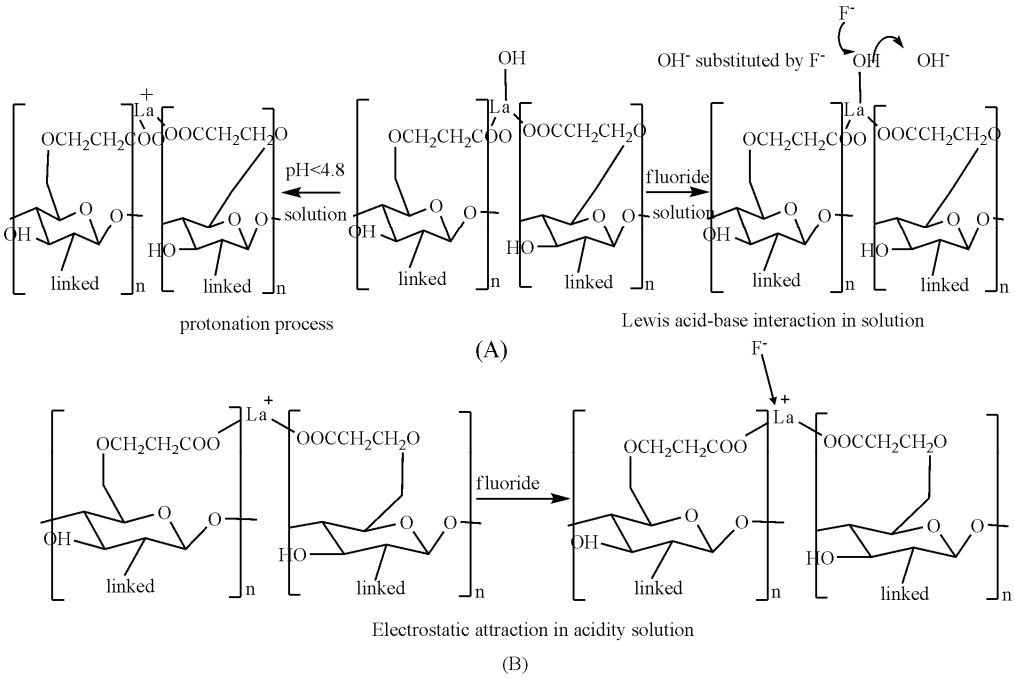

Fig.16. Scheme 2. Adsorption mechanism of fluoride onto linked CMC loaded with La (III) (A: Lewis acid-base interaction in solution, B: Electrostatic attraction in acidity solution.)

As NaOH was used as the eluent, hydroxyl ion may participate in the desorption process. The desorption mechanism analysis was shown in Fig. 17 Scheme 3A.

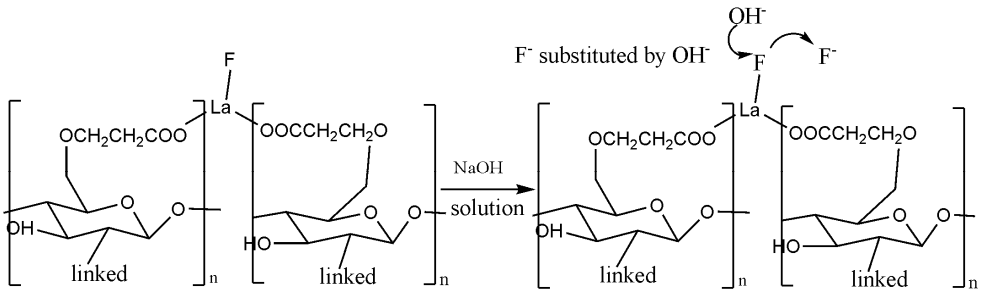

(A)

Fig.17. Scheme 3. Desorption mechanism of fluoride off linked CMC loaded with La (III)

4. Conclusions

In this study, carboxymethyl cellulose microsphere loaded with La (III) and linked carboxymethyl cellulose microsphere loaded with La (III) were fabricated and used to remove fluoride from aqueous solution. The adsorption property of CMC-La and linked CMC-La were investigated under batch experiments, and the crosslinking adsorption and desorption mechanism were analyzed. Conclusions can be summarized as follows:

(a) Compared with CMC-La, the linked CMC-La showed a better deed in **c**ompressive resistance, acid and alkali resistance and thermostability. The glutaraldehyde linking improved the adsorbent properties.

(b) The maximum removal efficiency of CMC-La and linked CMC-La were about 98 % and 99 %, respectively and both of them declined with the increase of the pH value. The kinetics model of adsorption belonged to pseudo-second order kinetic model.

(c) Linking process happened between hydroxyl of carboxylmethylcellulose and glutaraldehyde. Carboxyl and La (III) were the functional groups in the adsorption process. La (III) was loaded onto the CMC through ion exchange of sodium. The

adsorption of fluoride onto CMC-La was cooperation of Lewis acid-base interaction and electrostatic attraction when the solution was acidity. And desorption of the adsorbent happened because of the hydroxyl ion substituted fluorine again.

Acknowledgement

This work was financially supported by special project (13zg610301). Analytical facilities mainly provided by Engineering Research Center of Biomass Materials, Ministry of Education.

References

[1] J.V. Kumar, M.E. Moss, Fluorides in dental public health programs, Dent. Clin. North Am. 52 (2008) 387-401.

[2] WHO (World Health Organization), Guidelines for Drinking Water Quality, World Health Organization, Geneva, 2004.

[3] M. Islam, R.K. Patel, Thermal activation of basic oxygen furnace slag and evaluation of its fluoride removal efficiency, Chem. Eng. J. 169 (2011) 68-77.

[4] P. Sehn, Fluoride removal with extra low energy reverse osmosis membranes: thress years of large scale field experience in Finland, Desalination. 223 (2008) 73-84.

[5] Z. Qiusheng, L. Xiaoyan, L. Bin, L. Xuegang, Fluoride adsorption from aqueous solution by aluminum alginate particles prepared via electrostatic spinning device, Chem. Eng. J. 256 (2014) 306-315.

[6] E. Akbar, S.O. Maurice, O. Aoyi, A. Shigeo, Removal of fluoride ions from aqueous solution at low pH using schwertmannite, J. Hazard. Mater. 152 (2008) 571-579.

479 [7] A. Tor, Removal of fluoride from water using anion-exchange membrane under
480 Donnan dialysis condition, J. Hazard. Mater. 141 (2007) 814–818.
481 [8] L.N. Ho, T. Ishihara, S. Ueshima, H. Nishiguchi, Y. Takita, Removal of fluoride
482 from water through ion exchange by mesoporous Ti oxohydroxide, J. Colloid. Interf.
483 Sci., 272 (2004) 399-403.
484 [9] S. Chatterjee, S. De, Adsorptive removal of fluoride by activated alumina doped
485 cellulose acetate phthalate (CAP) mixed matrix membrane, Sep. Purif. Technol. 125
486 (2014) 223-238
487 [10] N. Kabay, O. Arar, S. Samatya, U. Yuksel, M. Yuksel, Separation of fluoride from
488 aqueous solution by electrodialysis: Effect of process parameters and other ionic
489 species, J. Hazard. Mater. 153 (2008) 107-113.
490 [11] A. Bhatnagar, E. Kumar, M. Sillanpää, Fluoride removal from water by
491 adsorption-A review, Chem. Eng. J. 171 (2011) 811-840.
492 [12] M. Mohapatra, K. Rout, P. Singh, S. Anand, S. Layek, H.C. Verma, B.K. Mishra,
493 Fluoride adsorption studies on mixed-phase nano iron oxides prepared by surfactant
494 mediation-precipitation technique, J. Hazard. Mater. 186 (2011) 1751-1757.
495 [13] A.M. Raichur, M.J. Basu, Adsorption of fluoride onto mixed rare earth oxides,
496 Sep. Purif. Technol. 24 (2001) 121-127.
497 [14] C.K. Rojas-Mayorga, A. Bonilla-Petriciolet, I.A. Aguayo-Villarreal, V.
498 Hemandez-Montoya, M.R. Moreno-Virgen, R.Tovar-Gómez, M.A.Montes-Morán,
499 Optimization of pyrolysis conditions and adsorption properties of bone char for
500 fluoride removal from water, J. Anal. Appl. Pyrol. 104 (2013) 10-18.

[15] R. Tovar-Gómez, M.R. Moreno-Virgen, J.A. Dena-Aguilar, V. Hernández-Montoya, A. Bonilla-Petriciolet, M.A. Montes-Morán, Modeling of fixed-bed adsorption of fluoride on bone char using a hybrid neural network approach, Chem. Eng. J. 228 (2013) 1098-1109.

[16] C.L. Yang, R. Dluhy, Electrochemical generation of aluminum sorbent for fluoride adsorption, J. Hazard. Mater. 94 (2002) 239-252.

[17] H. Deng, X. Yu, Adsorption of fluoride, arsenate and phosphate in aqueous solution by cerium impregnated fibrous protein, Chem. Eng. J. 184 (2012) 205-212.

[18] A. Teutli-Sequeira, V. Martínez-Miranda, M. Solache-Ríos, I. Linares-Hernández, Aluminum and lanthanum effects in natural materials on the adsorption of fluoride ions, J. Fluorine Chem. 148 (2013) 6-13.

[19] Y. Zhou, C. Yu, Y. Shan, Adsorption of fluoride from aqueous solution on La^{3+}-impregnated cross-linked gelatin, Sep. Purif. Technol. 36 (2004) 89-94.

[20] A. Bansiwal, D. Thakre, N. Labhshetwar, S. Meshram, S. Rayalu, Fluoride removal using lanthanum incorporated chitosan beads, Colloid Surface B. 74 (2009) 216-224.

[21] R.C. Oliveira, P. Hammer, E. Guibal, J. Taulemesse, O.G. Jr., Characterization of metal-biomass interactions in the lanthanum (III) biosorption on Sargassum sp. using SEM/EDX, FTIR, and XPS: Preliminary studies, Chem. Eng. J. 239 (2014) 381-391.

[22] F. Luo, K. Inoue, The removal of fluoride ion by using metal (III)-loaded amberlite resins, Solv. Ext. and Ion Exch. 22 (2004) 305–322.

[23] J. Chen, J. Wang, X. Zhang, Y. Jin, Microwave-assisted green synthesis of silver

523 nanoparticles by carboxymethyl cellulose sodium and silver nitrate, Mater. Chem.
524 Phys. 108 (2008) 421-424.
525 [24] N. Viswanathan, S. Meenakshi, Role of metal ion incorporation in ion exchange
526 resin on the selectivity of fluoride, J. Hazard. Mater. 162 (2009) 920–930.
527 [25] J. Wang, X.Y. Lin, X.G. Luo, Y.F. Long, A sorbent of carboxymethyl cellulose
528 loaded with zirconium for the removal of fluoride from aqueous solution, Chem. Eng.
529 J. 252 (2014) 415-422.
530 [26] M. Taniwaki, K. Kohyama, Mechanical and acoustic evaluation of potato chip
531 crispness using a versatile texture analyzer, J. Food Eng. 112 (2012) 268-273.
532 [27] X. Lin, J. Zhang, X. Luo, C. Zhang, Y. Zhou, Removal of aniline using lignin
533 grafted acrylic acid from aqueous solution, Chem. Eng. J. 172 (2011) 856-863.
534 [28] Q. Wu, J. Chen, M. Clark, Y. Yu, Adsorption of copper to different biogenic
535 oyster shell structures, Appl. Surf. Sci. 311 (2014) 264-272.
536 [29] I. Genta, M. Costantini, A. Asti, B. Conti, L. Montanari, Influence of
537 glutaraldehyde on drug release and mucoadhesive propertites of chitosan
538 microspheres, Carbohydr. Polym. 36 (1998) 81-88.
539 [30] S. Wu, D. Shen, J. Hu, R. Xiao, H. Zhang, TG-FTIR and Py-GC–MS analysis of
540 a model compound of cellulose - glyceraldehydes, J. Analy. Apply. Pyroly. : 101
541 (2013) 79–85.
542 [31] H.N. Umh, Y. Kim, Sensitivity of nanoparticles' stability at the point of zero
543 charge (PZC), J. Ind. Eng. Chem. 20 (2014) 3175-3178.
544 [32] J.A. Arcibar-Orozco, D. Josue, J.C. Rios-Hurtado, J.R. Rangel-Mendez,

545 Influence of iron content, surface area and charge distribution in the arsenic removal
546 by activated carbons, Chem. Eng. J. 249 (2014) 201-209.
547 [33] A.J. Varma, S.V. Deshpande, J.F. Kennedy, Metal complexation by chitosan and
548 its derivatives: a review, Carbohy. Polym. 55 (2004) 77-93.
549 [34] M. Figueiredo, A. Fernando, G. Martins, J. Freitas, F. Judas, H. Figueiredo, Effect
550 of the calcination temperature on the composition and microstructure of
551 hydroxyapatite derived from human and animal bone, Ceram. Int. 36 (2010)
552 2383-2393.
553 [35] H. Liu, F. Yang, Y. Zheng, J. Kang, J. Qu, J.P. Chen, Improvement of metal
554 adsorption onto chitosan/Sargassum sp. composite sorbent by an innovative
555 ion-imprint technology, Water Res. 45 (2011) 145-154.
556 [36] A. Masek, E. Chrzescijanska, A. Kosmalska, M. Zaborski, Characteristics of
557 compounds in hops using cyclic voltammetry, UV-VIS, FTIR and GC-MS analysis,
558 Food Chem. 156 (2014) 353-361.
559 [37] B. Grabowska, M. Sitarz, E. Olejnik, K. Kaczmarska, FT-IR and FT-Raman
560 studies of cross-linking processes with Ca^{2+} ions, glutaraldehyde and microwave
561 radiation for polymer composition of poly(acrylic acid)/sodium salt of carboxymethyl
562 starch - Part I, Spectrochim Acta A. 135 (2015) 529-535.
563 [38] Y.S. Ho, Removal of copper ions from aqueous solution by tree fern, Water Res.
564 37 (10) (2003) 2323–2330.

565 [39] K.G. Bhattacharyya, A. Sharma, Kinetics and thermodynamics of Methylene
566 Blue adsorption on Neem (Azadirachta indica) leaf powder, Dyes Pigments 65 (2005)
567 51–59.
568 [40] O. Aksakal, H. Ucun, Equilibrium, kinetic and thermodynamic studies of the
569 biosorption of textile dye onto Pinus sylvestrisL., J. Hazard. Mater. 181 (2010)
570 666-672.
571 [41] L. Poon, L. D. Wilson, J. Headley, Chitosan-glutaraldehyde copolymers and their
572 sorption properties, Carbohy. Polym. 109 (2014) 92-101.
573 [42] D. Pratt, L.D. Wilson, J.A. Kozinski, Preparation and sorption studies of
574 glutaraldehyde cross-linked chitosan copolymers, J. Colloid Interf. Sci. 395 (2013)
575 205-211.
576 [43] A. Heidari, H. Younesi, A. Rashidi, A.A. Ghoreyshi, Evaluation of CO_2
577 adsorption with eucalyptus wood based activated carbon modified by ammonia
578 solution through heat treatment, Chem. Eng. J. 254 (2014) 503-513.
579 [44] J. Feng, Z. Yang, G. Zeng, J. Huang, H. Xu, Y. Zhang, S. Wei, L. Wang, The
580 adsorption behavior and mechanism investigation of Pb(Ⅱ) removal by flocculation
581 using microbial flocculant GA1, Bioresource Technol. 148 (2013) 414-421.
582 [45] B. Liu, D. Wang, G. Yu, X. Meng, Removal of F- from aqueous solution using Zr
583 (Ⅳ) impregnated dithiocarbamate modified chitosan beads, Chem. Eng. J. 228 (2013)
584 224-231.
585 [46] I.P. Gustafsson, M. Akram, C. Tiberg, Predicting sulphate adsorption/desorption
586 in forest soils: Evaluation of an extended Freundlich equation, Chemosphere. 119

587 (2015) 83-89.

588 [47] S. Liu, Y. Ding, P. Li, K. Diao, X. Tan, F. Lei, Y. Zhan, Q. Li, B. Huang, Z.
589 Huang, Adsorption of the anionic dye Congo red from aqueous solution onto natural
590 zeolites modified with N,N-dimethyl dehydroabietylamine oxide, Chem. Eng. J. 248
591 (2014) 135-144.

592 [48] S. Zhang, Y. Lu, X. Lin, X. Su, Y. Zhang, Removal of fluoride from groundwater
593 onto La-Al loaded scoria adsorbent, Appl. Surf. Sci. 303 (2014) 1–5.

594 [49] S. Kamble, S. Jagtap, N. Labhsetwar, D. Thakare, S. Godfrey, S. Devotta, S.
595 Rayalu, Defluoridation of drinking water using chitin, chitosan and
596 lanthanum-modified chitosan, Chemical Engineering Journal, 129 (2007) 173–180.

597 [50] N. Viswanathan, C. S. Sundaram and S. Meenakshi, Removal of fluoride from
598 aqueous solution using protonated chitosan beads, J. Hazard. Mater., 161 (2009)
599 423–430.

600 [51] H. Paudyal, B. Pangeni, K. Ghimire, Adsorption behavior of orange waste gel for
601 some rare earth ions and its application to the removal of fluoride from water, Chem.
602 Eng. J., 195 (2012) 289–296.

603 [52] E. Kumar, A. Bhatnagar, M. Ji, W. Jung, S.-H. Lee, S. Kim, G. Lee, H. Song, J.
604 Choi, J. Yang, B. Jeon, Defluoridation from aqueous solutions by granular ferric
605 hydroxide (GFH), Water Res. 43 (2009) 490–498.

606 [53] H. Cai, G. Chen, C. Peng, Z. Zhang, Y. Dong, G. Shang, X. Zhu, H. Gao, X. Wan,
607 Removal of fluoride from drinking water using tea waste loaded with Al/Fe oxides: A
608 novel, safe and efficient biosorbent, App. Surf. Sci. 328 (2015) 34-44.

609 [54] J. Wang, D. Kang, X. Yu, M. Ge, Y. Chen, Synthesis and characterization of
610 Mg-Fe-Al trimetal composite as an adsorbent for fluoride removal, Chem. Eng. J. 264
611 (2015) 506-513.
612 [55] J. Han, S. Bourgeois, M. Lacroix, Protein-based coatings on peanut to minimize
613 oil migration, Food Chem. 115 (2009) 462-468.
614 [56] J. Shang, Z. Shao, X. Chen, Chitosan-based electroactive hydrogel, Polymer 49
615 (2008) 5520-5525.
616 [57] E. Emregul, O. Kocabay, B. Derkus, T. Yumak, K. Emregul, A. Sinag, K. Polat, A
617 novel carboxymethylcellulose-gelatin-titanium dioxide-superoxide dismutase
618 biosensor; electrochemical properties of carboxymethylcellulose-gelatin-titanium
619 dioxide-superoxide dismutase, Bioelectrochemistry, 90 (2013) 8-17.
620 [58] D. Thakre, S. Jagtap, A. Bansiwal, N. Labhsetwar, S. Rayalu, Synthesis of
621 La-incorporated chitosan beads for fluoride removal from water, J. Fluor. Chem. 131
622 (2010) 373-377.